Two Distinct Fetal-Type Signatures Caracterise Juvenile Myelomonocytic Leukemia

Marion Strullu
INSERM U1131
Chloé Arfeuille
INSERM 1131
Aurélie CAYE-EUDE
INSERM U1131
Loïc Maillard
INSERM U1131
Elodie Lainey
Assistance Publique -Hopitaux De Paris
Florian Piques
INSERM U1131
Odile Fenneteau
Hôpital Robert Debré
Cassinat Bruno
Assistance Publique Hopitaux de Paris
Guimiot Fabien
13Unité de Foetopathologie, Assistance Publique-Hôpitaux de Paris, CHU
Jean-Hugues Dalle
Hôpital Robert Debré
André Baruchel
Hopital Robert Debré
Christine Chomienne
INSERM U1131
Dominique Bonnet
The Francis Crick Institute https://orcid.org/0000-0002-4735-5226
Michele Souyri
Inserm U1156. CNRS UMR7622
Helene Cave (helene.cave@aphp.fr)
CHU-Paris - Hôpital Robert Debré, APHP https://orcid.org/0000-0003-2840-1511

Article

Keywords: Juvenile myelomonocytic leukemia, myeloproliferative neoplasm, fetal development, PTPN11, KRAS, LIN28B, inflammasome, hematopoietic progenitors

Posted Date: March 10th, 2022

DOI: https://doi.org/10.21203/rs.3.rs-1416605/v1

Abstract

To investigate whether ontogeny-related features determine the pediatric specificity in juvenile myelomonocytic leukemia (JMML), we compared the gene expression profile of hematopoietic progenitor cells sorted from JMML to their healthy counterparts isolated at different stages of ontogeny. Two groups of JMML were identified. The JMML in the first group had a fetal-like expression profile. Their progenitors showed a stronger monocytic identity than other JMML or healthy postnatal progenitors with overexpression of monocytic/dendritic, inflammasome and innate immunity markers, reminiscent of the monocyte-biased myelopoiesis characterizing physiologic fetal hematopoiesis. The second group, although clustering apart from healthy prenatal and post-natal fractions, was characterized by aberrant expression of the master oncofetal regulator *LIN28B*, suggesting developmental dysregulation. *LIN28B* expression was associated with DNA hypermethylation. Analysis of a large cohort of 108 patients with JMML showed that a high LIN28 expression was correlated to a poor outcome.

Our findings highlight a strong but complex link between JMML and development, and will be important to guide future treatment strategies in this rare but severe leukemia.

Key Points

- JMML is a transcriptionally heterogeneous disease with a strong fetal identity conferred by 2 distinct signatures
- A subset of JMML retains a physiologic fetal monocytic bias with an inflammasome signature in hematopoietic progenitors
- A distinct group of JMML shows aberrant expression of the oncofetal *LIN28B* master gene, DNA-hypermethylation and poor outcome.

Introduction

Juvenile myelomonocytic leukemia (JMML) is a clonal aggressive myeloproliferative and myelodysplastic neoplasia affecting infants and young children. It is characterized by splenomegaly, leukocytosis with precursors in peripheral blood and monocytosis, infiltration of peripheral tissues with histiocytes, but normal or only moderately increased blast count (1, 2). Allogeneic hematopoietic stem cell transplantation (HSCT) is the only curative therapy in JMML, which nonetheless has a 5-year overall survival rate of only 52% (3, 4). JMML is associated with constitutive activation of the RAS signaling pathway most often due to somatic gain-of-function mutations in *NRAS*, *KRAS* or *PTPN11* (encoding SHP2) (5). Recent studies have taken a major step forward in understanding the genomic and epigenetic underpinnings of JMML. Whole exome sequencing have uncovered that despite their aggressiveness, JMML has one of the lowest rate of mutations among cancers (6), and showed the association between JMML outcome and mutational profile (6–8). Furthermore, genome-wide DNA methylation analyses have identified a high-methylation subgroup displaying a high incidence of *PTPN11* mutations and poor clinical outcome (9–11).

Despite these major achievements many conundrums are yet to be answered. Why is the age-window so narrow? How can such an aggressive cancer develop with so few driving mutations? We hypothesized that these features could be related to the developmental nature of JMML. Indeed, the young age of patients at JMML onset is in favor of a prenatal initiation of JMML, a hypothesis confirmed by the identification of initiating mutations in cord blood and Guthrie card samples of some patients (12, 13). This suggests that developmental features are essential for JMML oncogenesis. The link between JMML and fetal development is further supported by features such as high expression of fetal hemoglobin (HbF) in a subset of JMML (14), and overexpression of *LIN28B* (15) a key developmental regulator that is highly expressed in fetal hematopoietic stem cell (HSC) (16) and controls the hemoglobin switch (17).

In contrast with adult hematopoiesis which takes place primarily in BM, fetal hematopoiesis occurs in multiple embryonic niches during development. After their emergence in the aorta/gonad/mesonephros region, HSC migrate to the fetal liver where they actively proliferate and expand, before fetal bone marrow (BM) colonization (18). Fetal hematopoietic progenitors are functionally distinct from adult progenitors and show differential intrinsic proliferation and differentiation potential according to gestational stage (16, 19, 20). For instance, human fetal CD34 + cells are more proliferative and self-renew extensively to build the blood system whereas adult HSC are quiescent. Thus, although fetal and adult HSCs share an overall biology, cell autonomous mechanisms based primarily on distinct transcriptional programs adapt their functions so as to best meet age-related needs, with a transcriptional switch occurring rapidly after birth (16, 19).

To determine whether the biology of JMML compares to that of embryo-fetal hematopoietic cells, we assessed immunophenotype and gene expression profile of JMML hematopoietic progenitor cells (HPC) in comparison with their healthy counterparts at different developmental stage, looking for transcriptional reminiscence of the normal compartment or JMML cell of origin.

We show here the major involvement of ontogeny-associated features in JMML and unveil a more complex picture than anticipated, with a fetal identity resulting either from retention of a physiologic fetal signature or from the aberrant activation of master oncofetal transcriptional regulators such as LIN28B. We also evidence high *LIN28B* expression as distinguishing a group of JMML with high DNA methylation and poor outcome.

Results

According to gene expression profile, most JMML HPC cluster either with embryo-fetal counterparts or in a JMML-dedicated group

To investigate whether gene expression profiling would identify a fetal transcriptional signature in JMML, we compared JMML of various genetic groups to healthy hematopoietic tissues obtained at different stages of ontogeny: fetal liver (FL), fetal bone marrow (FBM), and age-matched children bone marrow (BM) (Supplementary Fig. 1).

Immunophenotypic comparison of sorted hematopoietic stem and progenitor cell (HSPC) fractions in JMML (n = 28), FBM (n = 6), FL (n = 13) and postnatal bone marrow (BM) samples from healthy children (n = 23) (Supplementary Fig. 2A) showed global preservation of the hematopoietic structure in JMML (21) but evidenced variations between samples (e.g. HSC tend to be over-represented in the FL CD34 + compartment whereas GMP are under-represented) (Fig. 1; Supplementary Fig. 3). To overcome the variability in representation of HSPC populations across samples, gene expression profile was performed on isolated HPC fractions. FACS-sorted CMP, GMP and MEP were analyzed by RNAseq in JMML (n = 16) and their normal counterparts sorted from FL (n = 3), FBM (n = 2) and BM from healthy children (n = 7) (Supplementary Fig. 1; Supplementary Table 1). Immunophenotyping and cell sorting of progenitor cell fractions from JMML and their healthy prenatal and post-natal control samples was validated by both transcriptional and functional (colony forming assay) analysis (Supplementary Fig. 2).

When restricted to healthy fractions analysis, unsupervised hierarchical clustering and primary component analysis (PCA) grouped the samples primarily by ontogeny and, to a lesser extent, by hematopoietic differentiation, especially postnatal samples (Supplementary Fig. 4A,B). *LIN28B* and related genes (*IGF2BP1, IGF2BP3, HBG1, HBG2*) were among the most differentially expressed genes between the prenatal and post-natal fractions (Supplementary Fig. 4C; Supplementary Table 2). GSEA confirmed the significant enrichment in healthy fetal HPC of a set of transcripts including *Lin28B* that were previously reported in a FL mouse HSC signature (15, 16) (Supplementary Fig. 4D; Supplementary Table 3).

When analyzing healthy and JMML samples together, unsupervised hierarchical clustering separated the samples into 4 groups (C1-4) (Fig. 2A). Primary clustering by ontogeny was maintained, with a first branching separating 14/15 healthy embryo-fetal fractions in C1. Healthy postnatal samples were further grouped according to their differentiation stage, with healthy post-natal CMP and MEP in C2, and GMP in C3 (Fig. 2A). Strikingly, most JMML fractions clustered either in C1 with embryo-fetal fractions (17/47 fractions from 8/16 patients) or in a separate group (C4) containing no healthy samples (23/47 samples from 10/16 patients). Only a few JMML fractions co-clustered with healthy BM and these were mainly GMP. Indeed, unlike CMP and MEP, the GMP signature sometimes overtook ontogeny or oncogenesis with 1 fetal and 5 JMML GMP clustering with healthy postnatal GMP in C3. Removal of a set of 941 proliferation- and cell cycle-associated transcripts (MSigDB_M2227) did not affect the clustering, indicating that the transcriptional proximity between some JMML and fetal HPC is not primarily driven by a higher proliferative state.

We then grouped JMML patients according to preferential clustering (i.e. highest number of cell fractions in C1 with embryofetal fractions, in C2-3 with normal postnatal fractions, or in C4, respectively). Two major groups were defined accordingly: one with JMML resembling embryo-fetal samples (Fetal-JMML, JMML_F; 6/16), and a JMML-specific group (Onco-JMML, JMML_O; 7/16) (Supplementary Table 1). Patients with JMML_O tended to be older, with a more severe presentation and elevated fetal hemoglobin levels. All *PTPN11*-mutated JMML classified in this group. Patients with JMML_F tended to be younger and to display less severe perturbations of hematological markers (higher platelet count, lower WBC

count, lower dysplastic features) and mostly (5/6) had *NRAS* or *KRAS* mutations (Table 1; Supplementary Table 1).

Table 1
Main clinical and hematological features of JMML patients with RNAseq analysis in total and by gene expression group

	JMML_F	JMML_O	Total
n	6	8	16
Sex Ratio (M/F)	5	4	12/4
Age at onset (years), median (min-max)	1.2 (0.2–3.3)	3.7 (0,4–8)	1.2 (0.1-8)
Peripheral blood, median (min-max)			
WBC count, x10^9/L	18.8 (7.1–102.0)	35.9 (13.0-59.4)	35.9 (7.1–102.0)
Monocyte count, x10^9/L	3.3 (1.7–35.7)	6.2 (1.2–9.6)	5.9 (1.2–35.7)
Hb, g/dl	8.3 (7.2–11.3)	10.1 (8.2–12.2)	9.7 (7.2–12.2)
Platelets count, x10^9/L	83.5 (15–396)	54 (24–122)	63 (15–396)
Patients with myeloid precursors in PB	5/6	7/8	14/16
Patients with blasts in PB	4/6	7/7	11/15
Circulating blasts in PB (%)	1 (0-7.5)	2 (1–10)	1 (0-7.5)
Bone marrow			
Blasts (%)	6.5 (2–22)	8 (3–38)	5.2 (2–38)
Dysplastic features	3/5	7/7	11/13
Karyotype			
Normal	3/6	7/7	12/15
Monosomy 7	2/6	0/7	2/15
Other clonal alteration	1/6	0/7	1/15
RAS pathway mutation			
NRAS	3/6	2/8	6/16
KRAS	2/6	0/8	3/16
PTPN11	0/6	5/8	5/16
Other	1/7	1/8	2/16

M: male ; F: female ; WBC : white blood cell ; Hb: hemoglobin ; HSCT: hematopoietic stem cell transplant ; LFU: last follow-up ; PB: peripheral blood ; SNV: single nucleotide variation ; CNV: copy number variation

	JMML_F	JMML_O	Total
Additional alterations			
ASXL1	1/6	1/8	2/16
SETBP1	0/6	0/8	0/16
JAK3	0/6	1/8	1/16
RAS double mutant	0/6	2/8	2/16
≥ 2 alterations (SNV, CNV)	3/6	4/8	7/16
Outcome, n (%)			
HSCT	3/6	7/8	11/16
Relapse after HSCT	1/3	0/7	1/16
Alive at last follow up	5/6	8/8	15/16

M: male ; F: female ; WBC : white blood cell ; Hb: hemoglobin ; HSCT: hematopoietic stem cell transplant ; LFU: last follow-up ; PB: peripheral blood ; SNV: single nucleotide variation ; CNV: copy number variation

Activation of monocytic, dendritic and inflammasome pathways characterize Fetal-JMML

To better understand the biological characteristics underpinning the differences between these two groups of JMML, we compared gene expression in JMML_F and JMML_O progenitor samples.

A total of 1052 genes were up-regulated in JMML_F when compared with JMML_O (Fig. 2B; Supplementary Table 2). Gene ontology (GO) analysis showed enrichment for genes associated with various cellular processes (Supplementary Fig. 5) but the top 20 up regulated genes of the JMML_F group was strikingly composed of components of the Pyrin inflammasome or inflammation, monocytic cell markers, and genes related to the cytoskeleton or extra-cellular matrix (Fig. 3A). Notably, these genes were also differentially upregulated in the whole C1 cluster (i.e. including embryo-fetal healthy samples) versus C4 (Fig. 3B). GSEA performed on MSigDB indexed pathways showed enrichment of 32/62 (52%), 294/485 (61%), and 61/95 (64%) genesets containing the terms ‘monocytes’, ‘dendritic’, and ‘inflammation’ respectively, confirming enrichment of HPC from the JMML_F group in genes engaged in these processes (Supplementary Table 4). Further analysis based on signatures classifying monocytes and dendritic cells (DC)(22) showed enrichment of JMML_F HPC in signatures of classic, non-classic and intermediate monocytes and all types of conventional DC (Supplementary Table 3). Genes related to pyrin inflammasome were among the top upregulated genes in fetal JMML. An inflammasome signature recently reported to associate with oncogenic *KRAS* (23) as well as 3/3 MSigDB-indexed inflammasome genesets were enriched in JMML_F as compared with both JMML_O or healthy postnatal BM (Fig. 3C;

Supplementary Tables 2 and 3), in line with KRAS-JMML clustering in this group. Monocytic and inflammasome markers were enriched in the JMML_F HPC when compared with JMML_O but also when compared with healthy post-natal HPC (Fig. 3C, Supplementary Table 2), confirming that the monocyte program is abnormally enriched in the JMML_F group.

Individual examination of monocytes, DC and inflammation-related genes in HSPC revealed that their expression is not found in HSC/MPP but restricted to the JMML_F progeny compartments (Fig. 3D, Supplementary Fig. 5). Some (*CD14, SCIMP, ARHGEF10L, CLEC10A*) were expressed in the fetal liver HPC, whereas others (*CD300E, MEFV*) were physiologically absent from both prenatal or postnatal HPC (Fig. 3D). A high level of correlation was found between transcripts (Fig. 3E), consistent with the activation of a physiological program. As we were able to confirm the transcriptional and functional identity of the sorted GMP by colony forming assays (Supplementary Fig. 2), this aberrant expression of monocytic markers in HPCs reflects the abnormal persistence in these progenitors of a fetal differentiation stage where such an early priming of the monocytic differentiation programme is physiological.

Up regulation of master oncofetal transcription factors is a key feature of the Onco-JMML group

Differential gene expression analysis evidenced only 230 up-regulated genes in JMML_O when compared with JMML_F (Fig. 2B; Supplementary Table 2).

In the JMML_O group, the 20 highest scoring gene sets evidenced by GO analysis were exclusively related to protein synthesis pathways (Supplementary Fig. 5). Unexpectedly, among the top 3 genes up-regulated in the Onco-JMML group vs the Fetal group were 2 master embryo-fetal transcription factors, *LIN28B* and *WT1* (Fig. 4A). Both are considered fetal oncogenes as they are frequently overexpressed in malignancies and induce reactivation of fetal pathways (24, 25). Little correlation was found between the expression of these 2 oncogenes or with the other top upregulated gene (Fig. 4B). However, GSEA confirmed the high enrichment of *LIN28B* (16, 26) and *WT1* (27) expression signatures in the JMML_O (Fig. 4C; Supplementary Table 2).

As part of the LIN28B-Let-7-HMGA2 axis, LIN28B determines the higher self-renewal potential of fetal HSC (16). Accordingly, the LIN28B signature was found enriched in JMML_O HPC in comparison with healthy postnatal fractions but not prenatal fractions (Supplementary Table 2). Interestingly, hyperexpression of *LIN28B* and *WT1* was also found in JMML HSC and MPP fractions (Fig. 4D) and stable across HPC, suggesting impaired transcriptional regulation both according to ontogeny and differentiation. Consistent with this global enrichment, let7 tended to be downregulated and top LIN28B targets (16) (*HMGA2*, *IGFBP2*, *IGFBP3*) upregulated in the Onco-JMML, with mean expression levels comparable to those found in embryo-fetal fractions (Fig. 4E). However, with a drop of expression in HPC, the expression pattern of *HMGA2* did not fully parallel that of *LIN28B* in JMML, and *IGF2BP1*, a LIN28B-related oncofetal regulator found as the most highly expressed in fetal HPC (Supplementary Fig. 4) was not expressed in Onco-

JMML (Fig. 4E), revealing partial discrepancy between the physiological LIN28B-driven fetal signature and that found in JMML.

WT1 is known to be upregulated in myeloid malignancies including acute myeloblastic leukemia (AML). GSEA showed significant depletion of a signature described as downregulated in AML, but did not enable to confirm enrichment of an AML signature in the JMML_O group when compared to JMML_F (28, 29) (Supplementary Table 3).

LIN28B expression is associated with DNA hypermethylation in JMML

In order to get further insight into epigenetic modifications that may cause aberrant re-activation of oncofetal genes, we studied genome-wide DNA methylation on mononucleated cells from the 16 JMML, healthy postnatal (n = 2) and fetal (n = 2) BM using reduced-representation bisulfite sequencing (RRBS) (Supplementary Fig. 1). Overall, JMML showed a slightly hypermethylated pattern as compared with normal samples with a subgroup displaying marked hypermethylation (Fig. 5A,B, Supplementary Fig. 6A). Two main JMML clusters ($Meth^{high}$ and $Meth^{low}$) were delineated according to the level of hypermethylation (Fig. 5A,B). Limiting the analysis to CPG overlapping with previously published signatures (30, 31) reproduced the clustering (Supplementary Fig. 6B,C). In $Meth^{high}$ JMML, genes hypermethylated, either at transcription start site or in gene bodies, showed enrichment of a PRC2 epigenetic signature (Supplementary Fig. 6D).

As expected from previous observations in both JMML (30, 32) and healthy HSPC (33), the correlation between DNA methylation and gene expression was weak in our patients. However, despite no strict correlation at the patient's level, integrative analysis of DNA methylation and gene expression evidenced in the $Meth^{high}$ JMML a signature reminiscent of the JMML_O group, with over-expression of *LIN28B, HBG2, HBG1, PTX4, LINC01684, CLECL1* and *WT1* (Supplementary Table 4) and enrichment of the *LIN28B* signature (Fig. 5E). In JMML, a strict correlation was observed between DNA hypermethylation and *LIN28B* expression both in HPC and total mononucleated cells (Fig. 5B,D).

Remarkably, this correlation between hypermethylation and *LIN28B* expression was not found in healthy fetal samples. In contrast to what was seen at the transcriptional level, the fetal/postnatal shift was not accompanied by major change in DNA methylation (Fig. 5A).

Epigenetic alterations resulting in alternative promoter usage with expression of a long *LIN28B* transcript were recently reported in medulloblastoma (34). Quantification of *LIN28B* transcripts showed that, regardless of the methylation status, JMML expressed the canonical short *LIN28B* transcript, like healthy samples, ruling out such an epigenetic mechanism in $LIN28B^{high}$ JMML (Supplementary Fig. 7).

Overall, these findings show that gene expression profiling and DNA methylation identify overlapping signatures in JMML, that both rank *LIN28B* as the top deregulated gene.

LIN28B expression is associated with a poor prognosis in JMML

Extending the study to a large prospective cohort of 108 JMML cases, we evidenced *LIN28B* overexpression in 37 (34%), with a significant enrichment in PTPN11-JMML (54% vs 18%) (Fig. 5F, Table 2). LIN28B^{high} JMML had a dismal presentation, with lower median platelet counts (50 vs 84 x10^{9}/L), and higher levels of HBF (median 32% vs 6%), despite older median age (3.1 vs 1 year) (Table 2). The outcome of *LIN28B*^{high} cases was significantly poorer than that of other JMML cases, with a 3-year overall survival rate of 48% (CI 95%: 33%-69%) versus 90% (CI 95%: 83% – 97% ($p < 0.0001$) (Fig. 5F).

Table 2
Main clinical and hematological features of JMML patients with LIN28B ddPCR analysis in total and by LIN28B expression group

	Total	*LIN28B*^{High}	*LIN28B*^{Low}	p
n	108	37	71	
Sex Ratio (M/F)	1,5 (66/43)	2,1 (25/12)	1,3 (41/31)	
Age at onset (years), median (min-max)	1,6 (0,05–15,7)	3,1 (0,7–15,7)	1,0 (0,05–15,7)	0,0238
Peripheral blood, median (min-max)				
WBC count, x10^9/L	25,1 (4,0-102,0)	23,7 (6,1–83)	26,0 (4,0-102,0)	
Monocyte count, x10^9/L	5,1 (0,9–35,7)	5,6 (1,5–15)	4,6 (0,9–35,7)	
Hb, g/dl	9,8 (4,3–13,1)	9,9 (6,4–13,1)	9,6 (4,3–13,1)	
Platelets count, x10^9/L	69,5 (7-663)	50 (12–375)	84 (7-663)	
HbF elevated for age (children > 6m)	52/74	36/36 (100%)	16/38 (42%)	< 0,0001
if elevated, (%), median (min-max)		32 (3–85)	6 (2–14)	< 0,0001
RAS pathway mutation				
NRAS	24 (22%)	7 (19%)	17 (24%)	ns
KRAS	17 (16%)	3 (8%)	14 (20%)	ns
PTPN11	33 (30%)	20 (54%)	13 (18%)	0,0003
NF1	10 (9%)	6 (16%)	4 (6%)	ns
CBL	17 (16%)	0 (0%)	17 (24%)	0,003
Other	7 (6%)	1 (3%)	6 (8%)	ns
Additional alterations				
ASXL1	11 (10%)	7 (19%)	4 (6%)	
SETBP1	7 (6%)	3 (8%)	4 (6%)	
JAK3	9 (8%)	7 (22%)	2 (3%)	
RAS double mutant	13 (12%)	9 (24%)	4 (6%)	

WBC: white blood cell; HbF: fetal hemoglobin; ns: non-significant; HSCT: hematopoietic stem cell transplantation

	Total	*LIN28B*^{High}	*LIN28B*^{Low}	p
Monosomy 7	16 (15%)	2 (5%)	14 (20%)	
≥ 1 additional alteration	41 (38%)	22 (60%)	19 (27%)	0,0018
Outcome, n (%)				
HSCT	74 (69%)	32 (86%)	42 (60%)	0,0034
Watch and Wait strategy	29 (27%)	0 (0%)	29 (41%)	< 0,0001
Relapse after HSCT	17 (16%)	13 (35%)	4 (6%)	0,0002
Alive at last follow up	81 (76%)	20 (54%)	62 (86%)	
Lost to Follow-Up	1 (1%)	1 (3%)	0 (0%)	

WBC: white blood cell; HbF: fetal hemoglobin; ns: non-significant; HSCT: hematopoietic stem cell transplantation

Altogether, these findings suggest that *LIN28B*^{high} is a surrogate for both HBF hyperexpression and DNA hypermethylation in JMML and provides a simple and useful prognostic tool to identify high-risk patients.

Discussion

According to a rising concept in childhood cancer (35, 36), ontogenic changes in hematopoietic hierarchy may determine pediatric specificity by providing a permissive environment to oncogenic variants and/or modulate the susceptibility to transformation, thus possibly accounting for the paucity of oncogenic events required for oncogenesis. Indeed, there is increasing awareness that a number of critical pathways and processes that regulate developmental hematopoiesis are subverted to drive the initiation and/or evolution of hematological malignancies, and more specifically pediatric ones. In JMML, the need for a prenatal environment to support oncogenesis is suggested by *in utero* initiation and narrow age-window of onset (12, 13). We therefore hypothesized that the distinct features of JMML as compared with adult MPN are in part due to the persistence of features specific to early human development. Interestingly, comparing the gene expression profile of JMML with that of healthy samples at different stages of ontogeny revealed considerable transcriptional heterogeneity and identified 2 main groups of JMML, both of which linked to fetal development by a distinct mechanism.

We identified one group of JMML resembling embryo-fetal healthy samples more than age-matched ones. To our surprise, what links these JMML to fetal hematopoiesis is not *LIN28B* expression, as previously hypothesized (26) but a strong monocyte differentiation program with a signature of innate immune response and pyrin inflammasome that normally disappears later in ontogeny but persists in these JMML. Noteworthy, this is not just a consequence of clonal myelomonocyte development since it is only found in another subgroup of JMML. Little is known about fetal monocytes and their variations

across ontogeny. However, unlike post-natal hematopoiesis, fetal myeloid progenitors do not produce granulocytes but are directed solely towards monocyte production, which is consistent with the upregulation of a subset of monocytic or inflammatory markers (e.g. CD14, SCIMP) in FL.

Oncogenic RAS mutations occurring *in utero* could prevent postnatal extinction of the transient-by-nature HPC inflammasome activation regulating fetal HSPC, leading to the postnatal persistence of a fetal-type differentiation characterized by a lineage output oriented towards the production of myelomonocytic cells with early monocytic priming of myeloid progenitors and accounting for the monocytic bias observed in JMML. The connection of these with a physiological developmental state could explain the propensity of these leukemia to regress spontaneously as the child grows, a typical feature of developmental cancers observed in 3 of the 6 JMML in this group.

Interestingly, a role for transient innate immune cells in establishing the HSC program has recently be evidenced, with inflammasome as an homeostatic regulator of developmental hematopoiesis (38, 39). Pyrin (encoded by *MEFV*), overexpressed in this group of JMML, elicits proinflammatory cytokine release including IL-1β, a key pro-inflammatory signal shown to directly accelerate cell division and myeloid differentiation of HSCs through precocious activation of a PU.1-dependent gene program. Although restricted to progenitors, the pyrin inflammasome activation could thus also affect the HSC compartment through transmission of an inflammatory signal.

If this mechanism was to be confirmed, it would suggest that anti-inflammatory or immunomodulatory therapeutic approaches could be of interest in this subset of JMML.

Strikingly, it was in a second group of JMML, typified by their leukemic nature rather than developmental origin, that deregulation of fetal master regulators such as *LIN28B* were identified as potential functional drivers of the disease. LIN28B, the reactivation of which is common during oncogenesis is a key developmental regulator highly expressed during human embryogenesis but down-regulated in most tissues after birth (16, 40). LIN28B is believed to promote the reprogramming of hematopoietic progenitors into a fetal-like state and thereby elevate HBF levels (41). *LIN28B* expression has been proposed to define a ‘fetal-like’ JMML subtype (26). However, our data suggests on the one hand that activation of the LIN28B-Let7-HMGA2 axis alone does not fully reactivate the normal fetal physiology and on the other hand, that *LIN28B* hyperexpression responds to a regulatory mechanism in the JMML that is distinct from that observed during physiological development. This is further supported by subtle differences in the transcriptional signature (e.g. the lack of expression in *LIN28B* expressing JMML of *IGF2BP1*, a major LIN28B target in fetal samples) (16). The lack of *LIN28B* transcriptional decrease along JMML HSPC differentiation and the strong association of DNA methylation and LIN28B expression in JMML, also contrast to what is observed in fetal healthy samples. These results challenge models of oncogenesis that postulate the origin of LIN28B expressing JMML from uncontrolled proliferation of a developmental remnant, as we would thus expect retention of a lineage signatures.

Oncogenesis is frequently accompanied by the reappearance of fetal antigens (42, 43). Stegarchis et al (44), by analyzing regulatory landscapes across ontogeny and oncogenesis proposed the concept of ‘dys-

differentiation', resulting from the misregulation of key developmental transcription factors in opposition to de-differentiation, which implies reversion to a previous physiological stage (44). By selectively recruiting regulatory elements such as LIN28B that are active at other developmental stages, leukemia cells revert to a "pseudoprimitive" dys-differentiated state that combines regulatory DNA features of embryonic cells with those of other developing lineages. As such, JMML cells deviate from normal development and can no longer be placed on Waddington's landscape. This hypothesis is further supported in JMML by a previous reported of erythroid epigenetic changes in KLF1 which leads to HBF overexpression through a different mechanism from that of healthy newborn (45).

Interestingly, DNA methylation studies identified *LIN28B* as the most hyperexpressed transcript in the hypermethylated JMML group (11). Together with the findings that *LIN28B* expressing JMML as well as JMML_O are enriched in patients with *PTPN11* mutated JMML, older age at diagnosis, and poor outcome ((15) and this study), and consistent with the low overall gene expression observed in our JMML_O, this suggests that our 'Onco-JMML' may correspond to the recently described poor prognostic hypermethylated JMML group (26, 46), hedding light on the underlying biology of this clinically relevant group of JMML.

In conclusion, our findings showcase the importance of fetal cues in JMML but unveil a more complex situation than expected with two alternative (and mutually exclusive ways) to keep/reactivate fetal pathways in JMML. This provides a striking example of how ontogeny-related features are involved in childhood oncogenesis. The underlying biological pathways revealed by this study could be of help to guide new therapeutical approaches in this dreadful disease.

Patients And Methods

Patients

The study included a total of 111 patients with JMML consecutively referred to our laboratory between 2004 and 2021, for whom an activating mutation of the RAS pathway was identified and RNA was available. Patients with a constitutional mutation of *PTPN11* (Noonan syndrome) were excluded. Main patients' features are detailed in Table 2.

The diagnosis of JMML was based on clinical and hematological findings, centrally reviewed cytomorphological examination of blood and BM smears and mutation screening. Fetal hemoglobin (HbF) dosage and karyotyping were systematically performed using standard procedures. All patients fulfilled the WHO JMML criteria (1).

Samples

Patient BM or blood samples were collected at diagnostic of JMML. BM of healthy age-matched children (n = 23; median age 5.2 yrs, Supplementary Fig. 1) were obtained from intra-familial BM transplantation donors. Mononuclear cells of JMML and healthy samples were isolated on a Ficoll gradient (Eurobio) and

used directly or stored frozen in DMSO for later use. Patients and/or parents' informed consent was obtained in compliance with French regulation rules. This study was approved by the institutional review board of "Hôpitaux Universitaires Paris Nord Val-de-Seine", Paris University, AP-HP), (IRB: 00006477), in accordance with the Helsinki declaration.

Human first-trimester fetal liver (FL) (7.5 to 12.5 weeks of gestation (WG) (n = 13), and human fetal BM (FBM) (13.5 to 22.2 WG) (n = 6) were obtained after voluntary, spontaneous or therapeutic abortions in compliance with French laws, and specific authorization of the French Biomedicine Agency.

Characteristics of samples and details of the analyses performed are shown in Supplementary Fig. 1.

Fetal liver preparation

Fetal liver (FL) were excised sterilely using microsurgery instruments and a dissecting microscope, in phosphate-buffered saline (PBS) supplemented with 10% heat-inactived fetal calf serum (FCS) (Dominique Dutscher). Fetal livers were then mechanically disrupted through 18, 23 and 26 gauge needles successively and treated for 30min at 37°C with type I collagenase (Sigma) (0.125% in PBS with 10% FCS). Cells clumps were removed on a 70µm nylon filter (Miltenyi Biotec), washed three times with Dulbecco's modified eagle medium (DMEM, Gibco, ThermoFischer), FCS 10% and quantified. FBM were mechanically disrupted and treated for 1 hr at 37C with type I collagenase (Sigma) (0.125% in PBS with 10% FCS). After washing, cell suspension was filtered through 70-mm nylon mesh and resuspended in DMEM supplemented with 10% FCS.

Phenotype and Isolation of HSPC

CD34 + cells were selected from mononucleated cells using the Easysep Human CD34 positive selection kit (StemCell Technologies, Vancouver, Canada) following the manufacturer's instructions. Cells were phenotyped on a BD FACSCanto™ II analyzer (BD Biosciences) using marker combinations that have been validated in fetal and adult bone marrow (47, 48): HSC $CD34^+CD38^-CD45RA^-CD90^+$, MPP $CD34^+CD38^-CD45RA^-CD90^-CD49f^-$, LMPP $CD34^+CD38^-CD45RA^+$, CMP $CD34^+CD38^+CD45RA^-CD135^+$, GMP $CD34^+CD38^+CD45RA^+CD135^+$ and MEP $CD34^+CD38^+CD45RA^-CD135^-$ (Supplementary Fig. 2). DAPI was added to the cell suspension before sorting to exclude dead cells. Sorting of HSC, MPP, CMP, GMP and MEP cell fractions was performed using the immunophenoytypic signatures used for phenotyping on a BD FACSAria II or III™ cell sorter (BD Biosciences, CA) operating in 4-way purity sort mode and collected into 1.5 ml microfuge tubes. Antibodies used for flow cytometry are listed in the Supplementary Table 5.

Colony-forming Cell assay

In vitro growth assays of sorted myeloid progenitors were performed by plating BM, peripheral blood mononucleated cells or 200 isolated HSPC obtained from JMML and healthy patients in semi-solid methylcellulose (H4435 StemCell Technologies Inc, Vancouver, Canada), as previously described (49). Colonies were scored and morphologically assessed on day 14 after plating.

Genomic DNA and RNA extraction

Genomic DNA was extracted from mononuclear cells and sorted cell fractions (when available) using a Qiagen Mini or Midi Kit (Qiagen Gmbh). RNA was extracted from mononuclear cells or sorted HSPC (1000 to 10000 cells) using the RNeasy Mini or Micro Kit (Qiagen). Concentrations were measured using a NanoDrop® (Thermo Scientific). cDNA was obtained by reverse transcription of 1 µg RNA with random hexamers, using standard procedures.

RNA sequencing

RNAseq was performed on sorted HSPC fractions (HSC, MPP, CMP, GMP, MEP) from 16 JMML patients (PTPN11-JMML, n = 5; KRAS-JMML, n = 3; NRAS-JMML, n = 6, other JMML, n = 2) and HPC fractions (CMP, GMP, MEP) of 14 healthy samples (5 FL, 2 FBM and 7 healthy children BM) (Supplementary Fig. 1). RNAseq was also conducted on total mononucleated cells in 13 of the JMML patients (Supplementary Fig. 1).

Libraries were prepared with TruSeq® Stranded Total RNASample preparation kit (Illumina) according to supplier's recommendations. Briefly the ribosomal RNA fraction was removed from 1µg of total RNA using the Ribo-Zero™ Gold Kit (Epicentre). Fragmentation was then achieved using divalent cations under elevated temperature to obtain approximately 300bp pieces. Double strand cDNA synthesis was performed using reverse transcriptase and random primers, Illumina adapters were ligated and cDNA library was PCR amplified for sequencing. Paired-end 75b sequencing was then carried out on a HiSeq4000 (Illumina). Quality of reads was assessed for each sample using FastQC (http://www.bioinformatics.babraham.ac.uk/projects/fastqc/). CMP, GMP and MEP obtained from fresh BM and frozen MNC from the same BM (JMML-20) were analyzed in parallel. Hierarchical clustering and PCA confirmed co-clustering indicating that the gene expression profile was not affected by the pre-analytical processing of the samples. The 3 duplicate samples were then removed from the analyses.

Sequence alignment and quantification of gene expression. A subset of 500,000 reads from each Fastq file was aligned to the reference human genome hg19/GRCh37 with tophat2 to determine insert sizes with Picard. Full Fastq files were aligned to the reference human genome hg19/GRCh37 with tophat2 (-p 24 -r 150 -g 2 –library-type fr-firststrand) (50). We removed reads mapping to multiple locations. We quantified gene expression using the full Gencode v26lift37. We used HTSeq (51) to obtain the number of reads associated to each gene in the Gencode v26lift37 database (restricted to protein-coding genes, antisense and lincRNAs). We used the Bioconductor *DESeq* package (52) to import raw HTSeq counts for each sample into R statistical software and extract the count matrix. After normalizing for library size, we normalized the count matrix by the coding length of genes to compute FPKM scores (number of fragments per kilobase of exon model and millions of mapped reads). Samples with abnormally elevated numbers of genes with FPKM > 2 (JMML_10_CMP) or < 0.5 (JMML_20_CSH, MO_9_CMP, JMML_4_MPP) were removed from further analyses.

Unsupervised analysis. We used the Bioconductor *edgeR* package (53) to import raw HTSeq counts into R statistical software, and compute normalized log2 CPM (counts per millions of mapped reads) using the TMM, weighted trimmed mean of M-values, as normalization procedure. The normalized expression matrix from the 5000 most variant genes (based on standard deviation) was used to classify the samples according to their gene expression patterns using principal component analysis (PCA), hierarchical clustering and consensus clustering. We used standard R functions to perform the PCA and hierarchical clustering (with Euclidean distance and Ward method). We used consensus clustering (Bioconductor *ConsensusClusterPlus* package) (54) to examine the stability of the clusters. We established consensus partitions of the data set in K clusters (for K = 2, 3, ..., 8), on the basis of 1,000 resampling iterations (80% of genes, 80% of sample) of hierarchical clustering, with Pearson's dissimilarity as the distance metric and Ward's method for linkage analysis. We used the cumulative distribution functions (CDFs) of the consensus matrices to determine the optimal number of clusters (K = 3 for instance), considering both the shape of the functions and the area under the CDF curves, as previously described (54).

Differential expression analysis. We used the Bioconductor *limma* package (55) to test for differential expression using the *voom* transformation. We only tested genes expressed in at least one sample (FPKM $\geq$ 0.1) to improve the statistical power of the analysis. We applied a *q*-value threshold of 0.1 to define differentially expressed genes, between clusters identified above, with a minimum log2FC of 1.5 for all comparisons.

Pathway enrichment analysis. Hypergeometric tests were used to identify gene sets from the MSigDB v7.4 database (56) over-represented among the lists of up- or down-regulated genes, correcting for multiple testing with the Benjamini-Hochberg procedure and filtering with q-value < 0.1.

We used gene set enrichment analysis software and the Molecular Signature Database (http://www.broad.mit.edu/gsea/) (56). Whole FPKM data were used as input. Genes were ranked by signal-to-noise ratio, and statistical significance was determined by 1000 phenotype mutations. Gene sets with a false discovery rate < 0.25 were considered significant. Gene sets used in the different analyses are listed in the Supplementary Table 4.

Reduced-representation bisulfite sequencing (RRBS)

Library preparation and sequencing. Quantitative and qualitative control of DNA was carried out by specific double-stranded fluorescence assay and gel migration. Preparation of RRBS libraries for 'paird-end' sequencing on Illumina® sequencer, with the Premium RRBS kit (Diagenode®), including an MspI enzymatic digestion step (targeting CCGG sites), size selection and bisulfite conversion. Paired-end sequencing of 2x100 bases on NovaSeq™6000 (Illumina®) produced an average of 35 million sequence pairs per library, i.e. 70 million sequences, i.e. 7Gb, +/-12% with an estimated conversion rate > 98.

Sequence alignment and quantification of DNA methylation. Quality of reads was assessed for each sample using FastQC (http://www.bioinformatics.babraham.ac.uk/projects/fastqc/). We used BS-Seeker2 (57) to map RRBS data to the Human hg38 genome and retrieve the number of methylated and

unmethylated cytosines at each covered CpG site. Methylation rates were then integrated across CpG island (CGI)-based and gene-based features. CGI-based features were defined as follows: CpG islands (from UCSC database), shores (2 kb on each side of the island) and shelves (2 kb on each side of the shores). DNA methylation outside CpG islands was analyzed by grouping CpG sites not located in CGI-based features every 100kb window. Gene-based features were defined based on Gencode v26 assembly. We calculated for each gene the methylation rate across the promoter region (TSS+/-500bp) and the gene body.

Unsupervised analysis. Methylation rates for CGI and 100kb windows covered at least 50 times were used to build a methylation matrix. The methylation matrix from the 1000 most variant features (based on standard deviation) was used to classify the samples according to their methylation patterns using principal component analysis (PCA) and hierarchical clustering (cosine distance, Ward.D method).

Differential methylation analysis. We compared methylation rates across all CGI-based and gene-based features (covered by at least 50 reads). Q-values were computed by comparing the number of methylated and unmethylated reads in each condition using a logistic regression with overdispersion correction, and the SLIM method for p value adjustment, as implemented in the methylKit package (58). We also calculated the methylation rate difference (delta) between each pair of test and reference sample. We considered as differentially methylated every region with a q-value < 0.05 and a methylation delta > 0.05 or <-0.05 in at least 80% of test-reference pairs.

Pathway enrichment analysis. We used hypergeometric tests to identify gene sets from the MSigDB v7 database (59) overrepresented among the lists of up- or down-regulated genes, correcting for multiple testing with the Benjamini-Hochberg procedure.

Droplet-digital PCR (ddPCR)

LIN28B mRNA was quantified by droplet digital PCR (ddPCR) using *TBP* as a reference transcript. (Supplementary Table 2). The ddPCR assay was performed on 5µl cDNA, using the QX200 AutoDG Droplet Digital PCR System (BioRad, Hercules, CA, USA) according to the manufacturer's protocol. *LIN28B* and *TBP* assays were run as non-competing duplex, using custom primers and probes (Supplementary Table 2). The QuantaSoft software (version 1.7.4; BioRad, Hercules, CA USA) was used to assign positive/negative droplets and convert counts into a number of copies/mL for the target and reference transcript. Only samples with more than 200 *TBP* copies/µl were further considered for quantitation. Target gene expression levels were expressed as a ratio of the number of target gene copies / *TBP* copies. JMML samples were stratified into high or low expression of *LIN28B* using a threshold of 0.2 and 0.01 for children below and above year respectively. Normal perinatal *LIN28B* expression values were assessed using non-leukemic controls aged 1 day to 3 months (n = 19).

Statistics

Differences between groups were tested using multivariable one-way and two-way ANOVA unpaired analysis corrected for multiple comparisons (multiple groups). All analyses were performed with Prism

software version 6.0 (GraphPad, La Jolla, CA, USA). Statistical significance was defined as p value < 0.05. Statistical value is provided in each Figure.

Statistical analyses were performed with R version 3.6.2. Overall survival was calculated from the date of diagnosis to the date of death. Distribution of overall survival in the different groups of cases was estimated by the Kaplan-Meier technique using the “survminer” R package (v 0.4.8). The differences between the Kaplan-Meier curves for different groups of cases were tested using the Log-Rank test comparing the groups.

Depositing dataset

RNA sequencing data are available via ArrayExpress database: http://www.ebi.ac.uk/arrayexpress, Accession number E-MTAB-xxx (TBD).

Declarations

ACKNOWLEDGEMENT

We gratefully thank Profs I Roberts, A Roy and A Mead (WIMM, Oxford) for insightful discussions. We thank patients’families and pediatric oncologists from the “Société Française de lutte contre les cancers et leucémies de l’enfant et de l’adolescent” (SFCE) for sending us patients samples. We thank Céline Vallot and E Letouzé (GeCo) for expert bioinformatics assistance. We thank the Center for Biological Resources (CRB-cancer) (BB-0033-00076) of the Robert Debré hospital. This work was supported in part by INCa and Canceropole Ile-de-France. MS is the recipient of a PhD scholarship funded by ITMO cancer.

Author contributions

Conceptualization: HC, MSo and DB; Methodology: MSt, CA, AC, LM, EL, HC, MSo and DB; investigation/resources: MSt, CA, AC, EL, FP, OF, BC, JHD, AB; writing original draft: MSt, CA, HC; writing review & editing: all authors; funding acquisition: HC; supervision: HC, MS.

DISCLOSURE OF Conflict of interest

The authors declare no conflict of interests.

References

1. Arber DA, Orazi A, Hasserjian R, Thiele J, Borowitz MJ, Le Beau MM, et al. The 2016 revision to the World Health Organization classification of myeloid neoplasms and acute leukemia. Blood. 19 mai 2016;127(20):2391–405.

2. Chang TY, Dvorak CC, Loh ML. Bedside to bench in juvenile myelomonocytic leukemia: insights into leukemogenesis from a rare pediatric leukemia. Blood. 16 oct 2014;124(16):2487–97.
3. Locatelli F, Niemeyer CM. How I treat juvenile myelomonocytic leukemia. Blood. 12 févr 2015;125(7):1083–90.
4. Locatelli F, Nöllke P, Zecca M, Korthof E, Lanino E, Peters C, et al. Hematopoietic stem cell transplantation (HSCT) in children with juvenile myelomonocytic leukemia (JMML): results of the EWOG-MDS/EBMT trial. Blood. 1 janv 2005;105(1):410–9.
5. Niemeyer CM, Flotho C. Juvenile myelomonocytic leukemia: who's the driver at the wheel? Blood. 7 mars 2019;133(10):1060–70.
6. Caye A, Strullu M, Guidez F, Cassinat B, Gazal S, Fenneteau O, et al. Juvenile myelomonocytic leukemia displays mutations in components of the RAS pathway and the PRC2 network. Nat Genet. nov 2015;47(11):1334–40.
7. Stieglitz E, Taylor-Weiner AN, Chang TY, Gelston LC, Wang Y-D, Mazor T, et al. The genomic landscape of juvenile myelomonocytic leukemia. Nat Genet. nov 2015;47(11):1326–33.
8. Sakaguchi H, Okuno Y, Muramatsu H, Yoshida K, Shiraishi Y, Takahashi M, et al. Exome sequencing identifies secondary mutations of SETBP1 and JAK3 in juvenile myelomonocytic leukemia. Nat Genet. août 2013;45(8):937–41.
9. Lipka DB, Witte T, Toth R, Yang J, Wiesenfarth M, Nöllke P, et al. RAS-pathway mutation patterns define epigenetic subclasses in juvenile myelomonocytic leukemia. Nat Commun. 19 2017;8(1):2126.
10. Stieglitz E, Mazor T, Olshen AB, Geng H, Gelston LC, Akutagawa J, et al. Genome-wide DNA methylation is predictive of outcome in juvenile myelomonocytic leukemia. Nat Commun. 19 2017;8(1):2127.
11. Murakami N, Okuno Y, Yoshida K, Shiraishi Y, Nagae G, Suzuki K, et al. Integrated molecular profiling of juvenile myelomonocytic leukemia. Blood. 05 2018;131(14):1576–86.
12. Behnert A, Meyer J, Parsa J-Y, Hechmer A, Loh ML, Olshen A, et al. Exploring the genetic and epigenetic origins of juvenile myelomonocytic leukemia using newborn screening samples. Leukemia [Internet]. 28 juin 2021 [cité 2 août 2021]; Disponible sur: http://www.nature.com/articles/s41375-021-01331-0
13. Matsuda K, Sakashita K, Taira C, Tanaka-Yanagisawa M, Yanagisawa R, Shiohara M, et al. Quantitative assessment of PTPN11 or RAS mutations at the neonatal period and during the clinical course in patients with juvenile myelomonocytic leukaemia. Br J Haematol. févr 2010;148(4):593–9.
14. Niemeyer CM, Arico M, Basso G, Biondi A, Cantu Rajnoldi A, Creutzig U, et al. Chronic myelomonocytic leukemia in childhood: a retrospective analysis of 110 cases. European Working Group on Myelodysplastic Syndromes in Childhood (EWOG-MDS). Blood. 15 mai 1997;89(10):3534–43.
15. Helsmoortel HH, Bresolin S, Lammens T, Cavé H, Noellke P, Caye A, et al. LIN28B overexpression defines a novel fetal-like subgroup of juvenile myelomonocytic leukemia. Blood. 3 mars 2016;127(9):1163–72.

16. Copley MR, Babovic S, Benz C, Knapp DJHF, Beer PA, Kent DG, et al. The Lin28b-let-7-Hmga2 axis determines the higher self-renewal potential of fetal haematopoietic stem cells. Nat Cell Biol. août 2013;15(8):916–25.
17. Basak A, Munschauer M, Lareau CA, Montbleau KE, Ulirsch JC, Hartigan CR, et al. Control of human hemoglobin switching by LIN28B-mediated regulation of BCL11A translation. Nat Genet. 2020;52(2):138–45.
18. Dzierzak E, Bigas A. Blood Development: Hematopoietic Stem Cell Dependence and Independence. Cell Stem Cell. 03 2018;22(5):639–51.
19. Pietras EM, Passegué E. Linking HSCs to their youth. Nat Cell Biol. août 2013;15(8):885–7.
20. Popescu D-M, Botting RA, Stephenson E, Green K, Webb S, Jardine L, et al. Decoding human fetal liver haematopoiesis. Nature. 2019;574(7778):365–71.
21. Caye A, Rouault-Pierre K, Strullu M, Lainey E, Abarrategi A, Fenneteau O, et al. Despite mutation acquisition in hematopoietic stem cells, JMML-propagating cells are not always restricted to this compartment. Leukemia. juin 2020;34(6):1658–68.
22. Villani A-C, Satija R, Reynolds G, Sarkizova S, Shekhar K, Fletcher J, et al. Single-cell RNA-seq reveals new types of human blood dendritic cells, monocytes, and progenitors. Science. 21 2017;356(6335).
23. Hamarsheh S, Osswald L, Saller BS, Unger S, De Feo D, Vinnakota JM, et al. Oncogenic KrasG12D causes myeloproliferation via NLRP3 inflammasome activation. Nat Commun. déc 2020;11(1):1659.
24. Copley MR, Eaves CJ. Developmental changes in hematopoietic stem cell properties. Exp Mol Med. 15 nov 2013;45:e55.
25. Parenti R, Salvatorelli L, Musumeci G, Parenti C, Giorlandino A, Motta F, et al. Wilms' tumor 1 (WT1) protein expression in human developing tissues. Acta Histochem. juin 2015;117(4–5):386–96.
26. Helsmoortel HH, Bresolin S, Lammens T, Cavé H, Noellke P, Caye A, et al. LIN28B overexpression defines a novel fetal-like subgroup of juvenile myelomonocytic leukemia. Blood. 3 mars 2016;127(9):1163–72.
27. Niavarani A, Herold T, Reyal Y, Sauerland MC, Buchner T, Hiddemann W, et al. A 4-gene expression score associated with high levels of Wilms Tumor-1 (WT1) expression is an adverse prognostic factor in acute myeloid leukaemia. Br J Haematol. févr 2016;172(3):401–11.
28. Roushangar R, Mias GI. Multi-study reanalysis of 2,213 acute myeloid leukemia patients reveals age- and sex-dependent gene expression signatures. Sci Rep. déc 2019;9(1):12413.
29. Bresolin S, Zecca M, Flotho C, Trentin L, Zangrando A, Sainati L, et al. Gene expression-based classification as an independent predictor of clinical outcome in juvenile myelomonocytic leukemia. J Clin Oncol. 10 avr 2010;28(11):1919–27.
30. Lipka DB, Witte T, Toth R, Yang J, Wiesenfarth M, Nöllke P, et al. RAS-pathway mutation patterns define epigenetic subclasses in juvenile myelomonocytic leukemia. Nat Commun. déc 2017;8(1):2126.

31. Schönung M, Meyer J, Nöllke P, Olshen AB, Hartmann M, Murakami N, et al. International Consensus Definition of DNA Methylation Subgroups in Juvenile Myelomonocytic Leukemia. Clin Cancer Res. 1 janv 2021;27(1):158–68.
32. Murakami N, Okuno Y, Yoshida K, Shiraishi Y, Nagae G, Suzuki K, et al. Integrated molecular profiling of juvenile myelomonocytic leukemia. Blood. 5 avr 2018;131(14):1576–86.
33. Farlik M, Halbritter F, Müller F, Choudry FA, Ebert P, Klughammer J, et al. DNA Methylation Dynamics of Human Hematopoietic Stem Cell Differentiation. Cell Stem Cell. 1 déc 2016;19(6):808–22.
34. Hovestadt V, Jones DTW, Picelli S, Wang W, Kool M, Northcott PA, et al. Decoding the regulatory landscape of medulloblastoma using DNA methylation sequencing. Nature. juin 2014;510(7506):537–41.
35. Lopez CK, Noguera E, Stavropoulou V, Robert E, Aid Z, Ballerini P, et al. Ontogenic Changes in Hematopoietic Hierarchy Determine Pediatric Specificity and Disease Phenotype in Fusion Oncogene-Driven Myeloid Leukemia. Cancer Discov. 2019;9(12):1736–53.
36. Roberts I, Fordham NJ, Rao A, Bain BJ. Neonatal leukaemia. Br J Haematol. 2018;182(2):170–84.
37. Matsuda K, Sakashita K, Taira C, Tanaka-Yanagisawa M, Yanagisawa R, Shiohara M, et al. Quantitative assessment of PTPN11 or RAS mutations at the neonatal period and during the clinical course in patients with juvenile myelomonocytic leukaemia. Br J Haematol. févr 2010;148(4):593–9.
38. Espin-Palazon R, Weijts B, Mulero V, Traver D. Proinflammatory Signals as Fuel for the Fire of Hematopoietic Stem Cell Emergence. Trends in Cell Biology. janv 2018;28(1):58–66.
39. Espín-Palazón R, Stachura DL, Campbell CA, García-Moreno D, Del Cid N, Kim AD, et al. Proinflammatory Signaling Regulates Hematopoietic Stem Cell Emergence. Cell. nov 2014;159(5):1070–85.
40. Yuan J, Nguyen CK, Liu X, Kanellopoulou C, Muljo SA. Lin28b Reprograms Adult Bone Marrow Hematopoietic Progenitors to Mediate Fetal-Like Lymphopoiesis. Science. 9 mars 2012;335(6073):1195–200.
41. Basak A, Munschauer M, Lareau CA, Montbleau KE, Ulirsch JC, Hartigan CR, et al. Control of human hemoglobin switching by LIN28B-mediated regulation of BCL11A translation. Nat Genet. févr 2020;52(2):138–45.
42. Viswanathan SR, Powers JT, Einhorn W, Hoshida Y, Ng TL, Toffanin S, et al. Lin28 promotes transformation and is associated with advanced human malignancies. Nat Genet. juill 2009;41(7):843–8.
43. Ahrlund-Richter L, Hendrix MJC. Oncofetal signaling as a target for cancer therapy. Semin Cancer Biol. déc 2014;29:1–2.
44. Stergachis AB, Neph S, Reynolds A, Humbert R, Miller B, Paige SL, et al. Developmental fate and cellular maturity encoded in human regulatory DNA landscapes. Cell. 15 août 2013;154(4):888–903.
45. Fluhr S, Krombholz CF, Meier A, Epting T, Mücke O, Plass C, et al. Epigenetic dysregulation of the erythropoietic transcription factor *KLF1* and the β-like globin locus in juvenile myelomonocytic leukemia. Epigenetics. 3 août 2017;12(8):715–23.

46. Flotho C. Gene mutations do not operate in a vacuum: the increasing importance of epigenetics in juvenile myelomonocytic leukemia. Epigenetics. 2019;14(3):236–44.
47. Notta F, Doulatov S, Laurenti E, Poeppl A, Jurisica I, Dick JE. Isolation of single human hematopoietic stem cells capable of long-term multilineage engraftment. Science. 8 juill 2011;333(6039):218–21.
48. Notta F, Zandi S, Takayama N, Dobson S, Gan OI, Wilson G, et al. Distinct routes of lineage development reshape the human blood hierarchy across ontogeny. Science. 8 janv 2016;351(6269):aab2116–aab2116.
49. Pérez B, Kosmider O, Cassinat B, Renneville A, Lachenaud J, Kaltenbach S, et al. Genetic typing of CBL, ASXL1, RUNX1, TET2 and JAK2 in juvenile myelomonocytic leukaemia reveals a genetic profile distinct from chronic myelomonocytic leukaemia: JMML and CMML Have Distinct Genetic Profile. British Journal of Haematology. déc 2010;151(5):460–8.
50. Kim D, Pertea G, Trapnell C, Pimentel H, Kelley R, Salzberg SL. TopHat2: accurate alignment of transcriptomes in the presence of insertions, deletions and gene fusions. Genome Biology. 25 avr 2013;14(4):R36.
51. Anders S, Pyl PT, Huber W. HTSeq–a Python framework to work with high-throughput sequencing data. Bioinformatics. 15 janv 2015;31(2):166–9.
52. Anders S, Huber W. Differential expression analysis for sequence count data. Genome Biol. 2010;11(10):R106.
53. Robinson MD, Oshlack A. A scaling normalization method for differential expression analysis of RNA-seq data. Genome Biology. 2 mars 2010;11(3):R25.
54. Monti S, Tamayo P, Mesirov J, Golub T. Consensus Clustering: A Resampling-Based Method for Class Discovery and Visualization of Gene Expression Microarray Data. Mach Learn. juill 2003;52(1–2):91–118.
55. Ritchie ME, Phipson B, Wu D, Hu Y, Law CW, Shi W, et al. limma powers differential expression analyses for RNA-sequencing and microarray studies. Nucleic Acids Res. 20 avr 2015;43(7):e47.
56. Subramanian A, Tamayo P, Mootha VK, Mukherjee S, Ebert BL, Gillette MA, et al. Gene set enrichment analysis: a knowledge-based approach for interpreting genome-wide expression profiles. Proc Natl Acad Sci USA. 25 oct 2005;102(43):15545–50.
57. Guo W, Fiziev P, Yan W, Cokus S, Sun X, Zhang MQ, et al. BS-Seeker2: a versatile aligning pipeline for bisulfite sequencing data. BMC Genomics. 10 nov 2013;14:774.
58. Akalin A, Kormaksson M, Li S, Garrett-Bakelman FE, Figueroa ME, Melnick A, et al. methylKit: a comprehensive R package for the analysis of genome-wide DNA methylation profiles. Genome Biol. 3 oct 2012;13(10):R87.
59. Subramanian A, Tamayo P, Mootha VK, Mukherjee S, Ebert BL, Gillette MA, et al. Gene set enrichment analysis: A knowledge-based approach for interpreting genome-wide expression profiles. Proceedings of the National Academy of Sciences. 25 oct 2005;102(43):15545–50.

Figures

Figure 1

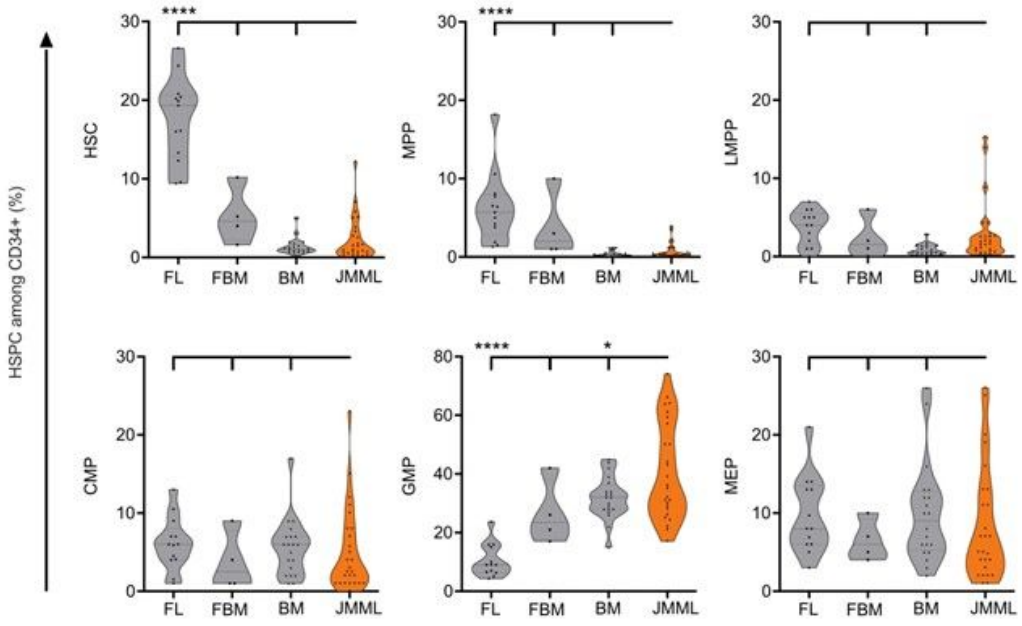

Figure 1

Frequency of immunophenotypically defined stem (HSC, MPP, LMPP; up panel), and progenitor (CMP, GMP, MEP; bottom panel) fractions within total $CD34^+$ cells in BM of patients with JMML (n=26) compared to their normal counterparts sorted from FL (n=13), FBM (n=4) and BM from healthy children (n=20). Medians are indicated by horizontal black lines. Anova multiple comparison, ****p<0.0001; *p <0.05. FL: Fetal liver; FBM: fetal bone marrow; BM: postnatal bone marrow.

Figure 2

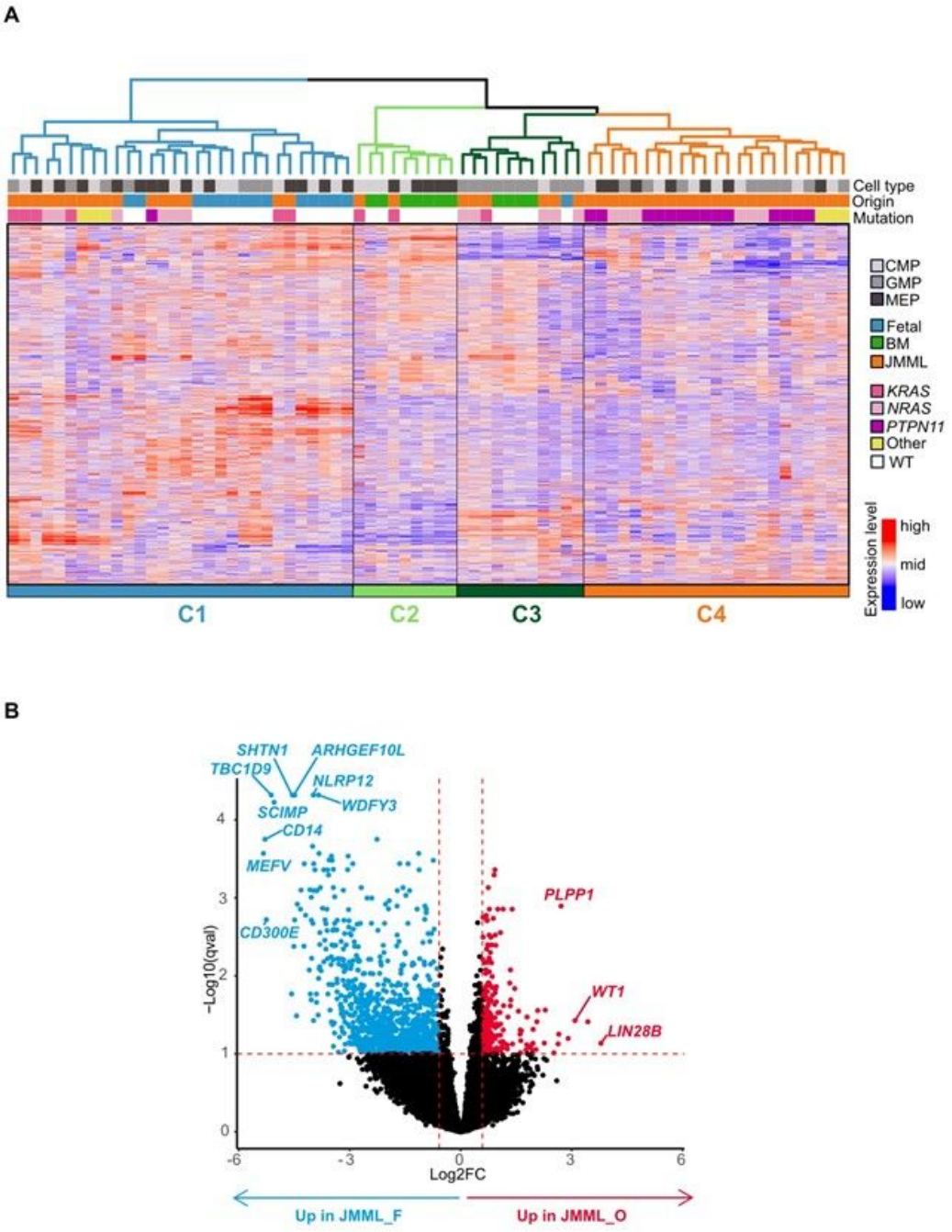

Figure 2

Gene expression profile of JMML progenitors versus healthy prenatal and postnatal counterparts. **(A)** Unsupervised hierarchical clustering of sorted JMML hematopoietic progenitors (CMP, GMP, MEP) and their pre- or post-natal counterparts according to gene expression profile. Four clusters (C1 to C4) were

defined. C1 contains FL samples (n= 9/9) FBM samples (5/6), and 16/47 JMML samples (CMP n=5, GMP n=3, MEP n=8) from 8/16 patients. C2 contains healthy BM, 7/7 samples (CMP n=3/3, MEP n=4/4), and 2 JMML samples (#12). C3 contains GMP from 4/4 healthy BM, 1/4 FBM, JMML GMP (5/16 samples) and 1 JMML CMP. C4 contains 23/47 JMML samples (CMP n=8, GMP n=8 and MEP n=7) from 10/16 patients and no healthy fetal or postnatal tissue (see also Supplementary Table 5). FL: Fetal liver; FBM: fetal bone marrow; BM: postnatal bone marrow. **(B)** Vulcano plot showing differentially expressed genes upregulated in JMML_F (left) or JMML_O (right) according to log2 fold change (x axis) and q-value (y axis). Differential gene expression analysis between JMML groups evidenced 1052 up-regulated genes with a fold change higher than 1.5 and a q-value lower than 0.1 in JMML_F versus 230 up-regulated genes in JMML_O (listed in Supplementary Table 2).

Figure 3

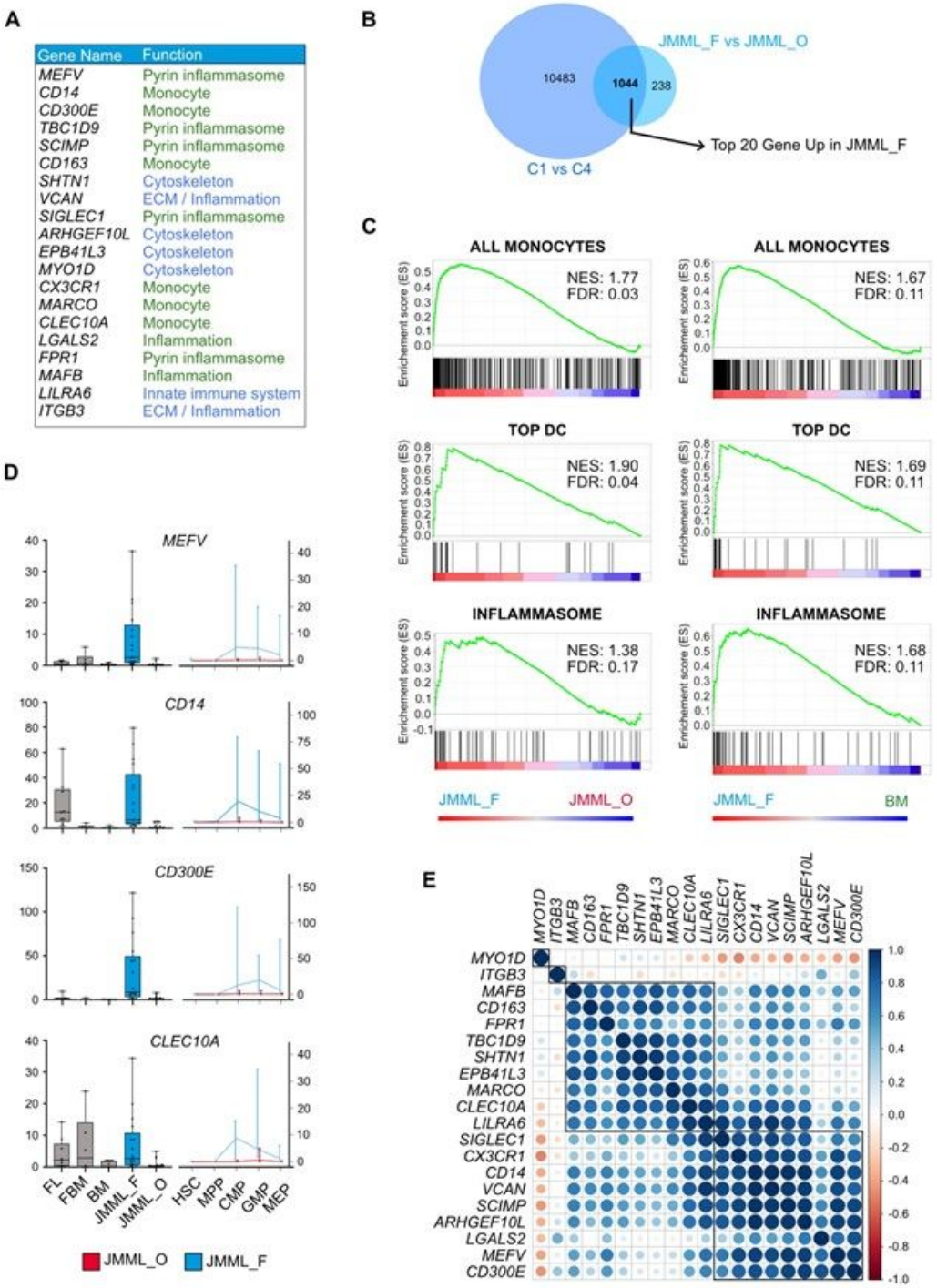

Figure 3

Gene expression profiling shows enrichment of monocyte and inflammasome markers in the JMML_F group. **(A)** List of the top 20 up-regulated genes in JMML from the JMML_F group with indication of their function in monocyte/inflammasome (in green) or cellular process (in blue). ECM: extra-cellular matrix. **(B)** Venn diagram illustrating the overlap between differentially expressed genes depending on whether cluster 1 (i.e. healthy fetal samples and JMML_F) or only the cluster 1-associated JMML samples

(JMML_F) is compared to cluster 4 (JMML_O). The top 20 differentially expressed genes in JMML_F vs JMML_O are also part of the differential signature between C1 and C4. **(C)** GSEA plots for gene signatures significantly enriched in JMML_F versus JMML_O (left panels) or versus healthy BM (right panels) (see also Supplementary Table 4). NES: Normalized enrichment score. FDR: false discovery rate. BM: postnatal bone marrow; DC: dendritic cell. **(D)** Histograms comparing gene expression (expressed as mean FPKM scores ±SD) in GMP of healthy samples across ontogeny (FL, FBM, BM), JMML_F and JMML_O (left panels); plots showing gene expression levels (FPKM) in sorted HSPC fractions (HSC, MPP, CMP, GMP, MEP) obtained from JMML_O (red) or JMML_F (blue) (right panels); see also Supplementary Figure 5. **(E)** Correlogram of the 20 most upregulated genes in the JMML_F group. FL: Fetal liver; FBM: fetal bone marrow; BM: postnatal bone marrow; FPKM: fragments per kilobase million.

Figure 4

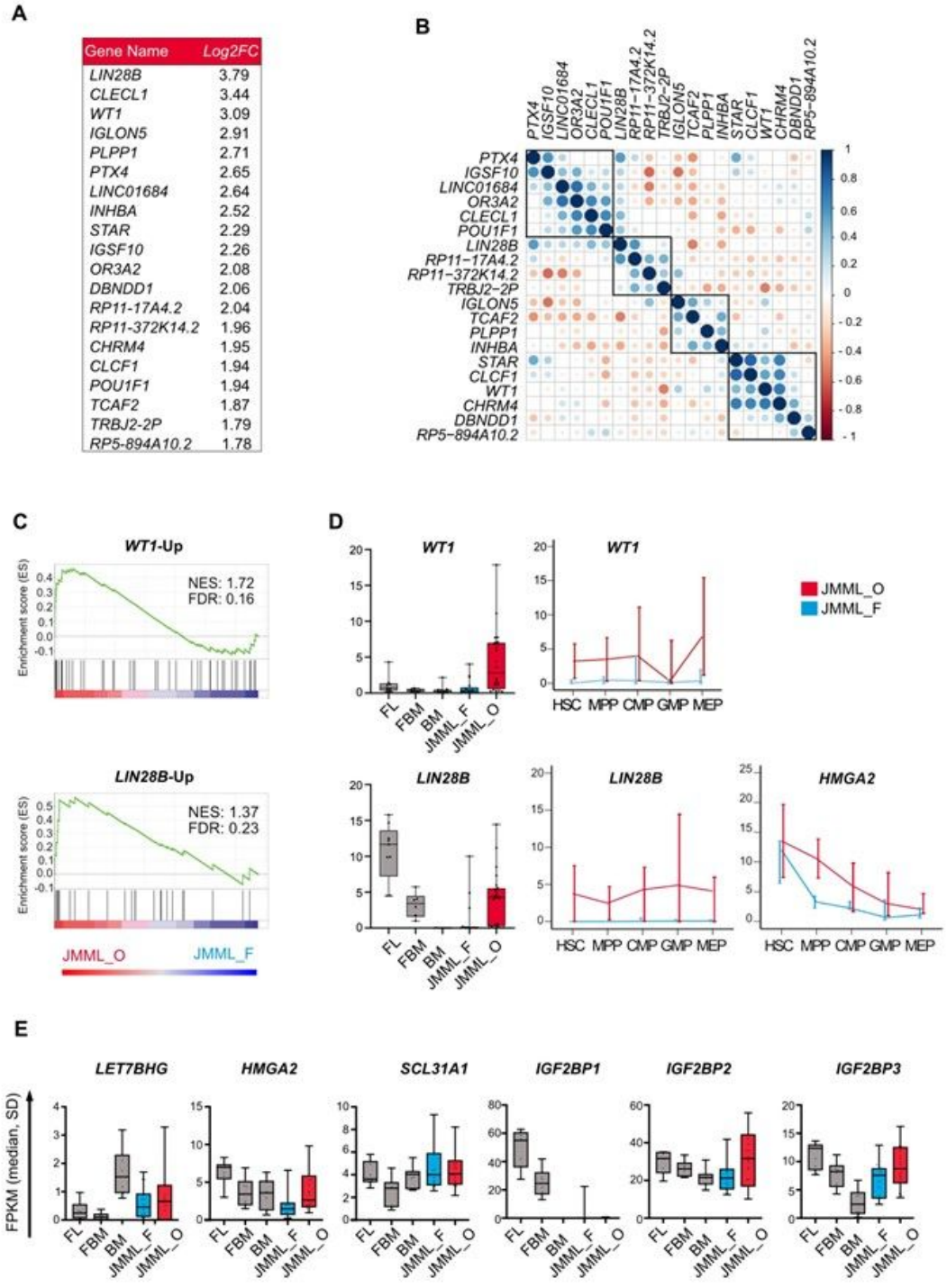

Figure 4

Gene expression profiling reveals expression of key oncofetal transcriptional regulators in the JMML_O group. **(A)** List of the top 20 up-regulated genes in JMML_O. **(B)** Correlogram between the expression of these 20 genes. **(C)** GSEA plots for gene signatures significantly enriched in JMML_O versus JMML_F. **(D)** Expression (FPKM) of *WT1* (upper panels) and *LIN28B* (bottom panels). Histograms comparing the gene expression (FPKM) in GMP across ontogeny (FL, FBM, BM) and in JMML_F and JMML_O groups (left

panels); plots showing gene expression levels (expressed as mean FPKM scores ±SD) in sorted HSPC fractions (HSC, MPP, CMP, GMP, MEP) obtained from JMML_O (red) or JMML_F (blue) groups (right panels). **(E)** Histograms comparing the gene expression level (FPKM) of key LIN28B targets in GMP across ontogeny (FL, FBM, BM), JMML_F and JMML_O groups (right panels). FL: Fetal liver; FBM: fetal bone marrow; BM: postnatal bone marrow; NES: Normalized enrichment score. FDR: false discovery rate; FPKM: fragments per kilobase million.

Figure 5

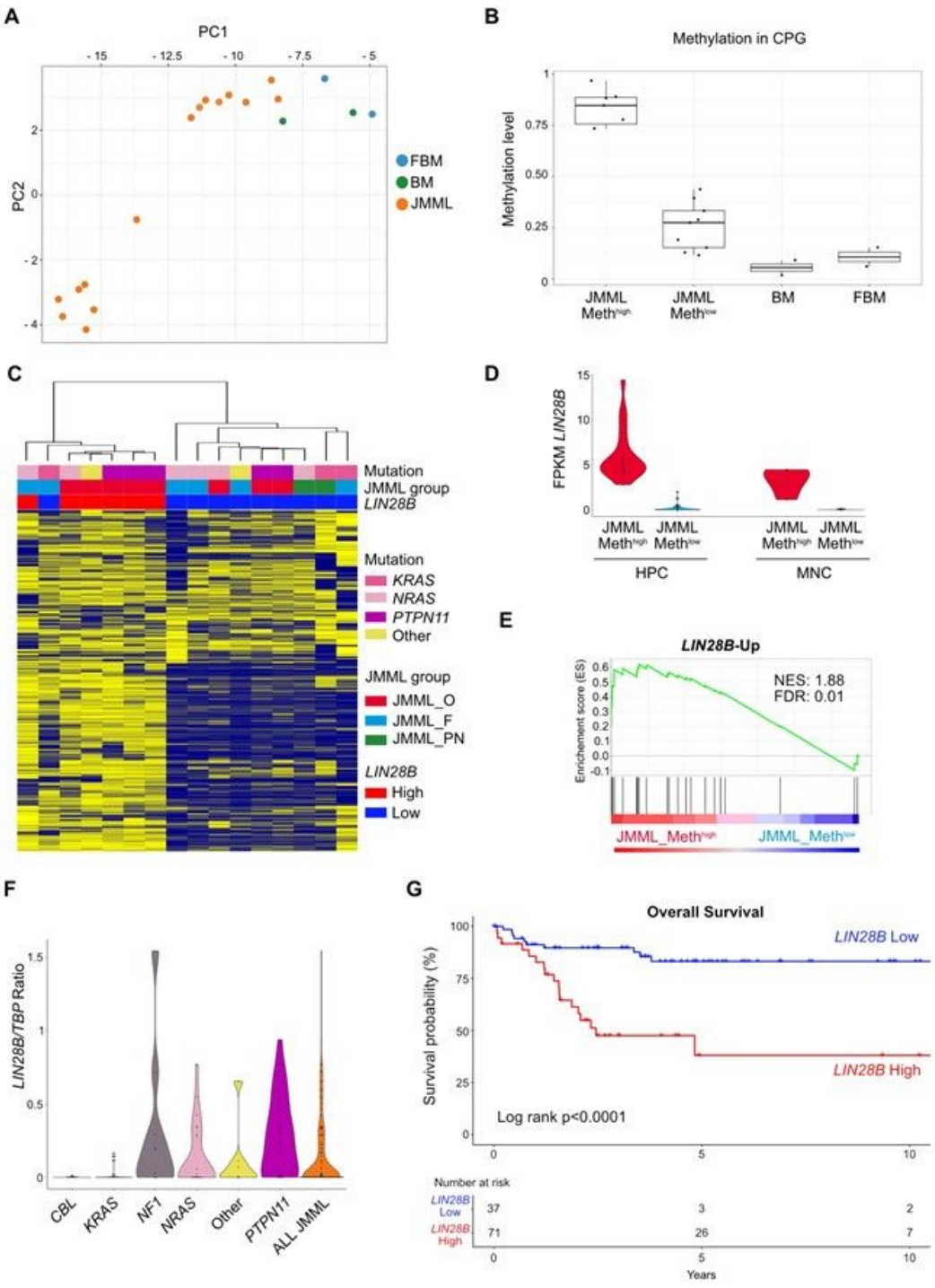

Figure 5

DNA methylation and *LIN28B* expression in JMML. **(A)** Principal component analysis (PCA) of DNA methylation data obtained by RRBS for mononucleated cells from JMML samples (n=16), fetal bone marrow (FBM; n=2), and healthy postnatal bone marrow (BM; n=2). The DNA methylation study distinguishes 3 groups of JMML according to low (Meth^{low}, n=8), intermediate (n=1), or high (Meth^{high}, n=6) level of methylation. **(B)** Unsupervised hierarchical clustering of JMML samples according to DNA

methylation data. **(C)** DNA methylation level measured in arbitrary units in JMML Meth^{high}, JMML Meth^{low}, BM and FBM. **(D)** *LIN28B* expression (FPKM) in Meth^{high} and Meth^{low} JMML progenitor fractions (HPC) or total moonucleated cells (MNC). **(E)** GSEA plot showing significant enrichment of the LIN28B signature in JMML Meth^{high} versus JMML Meth^{low}. **(F)** *LIN28B* transcript expression measured by ddPCR in the whole cohort of JMML (ALL JMML; n=108), and by genetic group. **(G)** Kaplan-Meier estimates of the overall survival of patients with JMML (n=108) according to the level of expression of the *LIN28B* transcript.

Supplementary Files

This is a list of supplementary files associated with this preprint. Click to download.

- StrulluSupplementaryFigures1.pptx
- StrulluSupplementaryFigures3.pptx
- StrulluSupplementaryFigures5.pptx
- StrulluSupplementaryFigures7.pptx
- StrulluSupplementaryFigures6.pptx
- StrulluSupplementaryFigures2.pptx
- StrulluSupplementaryFigures4.pptx
- StrulluTable1.docx
- StrulluSupplementaryTable5.docx
- StrulluSupplementaryTable3.docx
- StrulluSupplementaryTable4.xlsx
- StrulluSupplementaryTable1.docx
- StrulluTable2.docx
- StrulluSupplementaryTable2.xlsx